# Bidirectional enhanced quantile gated recurrent unit for short-term forecasting of PM2.5 with emphasis on extreme events in Sri Lanka

**Short title:** Quantile based deep learning for extreme PM2.5 forecasting

J. M. V. Anjana B. Jayasinghe

Department of Statistics, Faculty of Science, University of Colombo, Colombo, Sri Lanka

Chandima D. Tilakaratne

Department of Statistics, Faculty of Science, University of Colombo, Colombo, Sri Lanka

*** Corresponding author. E-mail:** anjana.jayasinghe1013@gmail.com

## Abstract

Air quality forecasting is critical for mitigating the health impacts of fine particulate matter (PM2.5). This study introduces a hybrid deep learning model, the bidirectional enhanced quantile gated recurrent unit (BEQ-GRU), for short-term forecasting of PM2.5 concentrations with explicit emphasis on extreme pollution occurrences. This model was applied to forecast PM2.5 levels in two high-risk Sri Lankan cities, Colombo and Kandy, delivering 24-hour and 48-hour ahead forecasts. Unlike conventional point-estimation models that optimise for mean accuracy, the BEQ-GRU targets the upper tail of the conditional distribution through an asymmetric quantile objective engineered to capture the heavy-tailed distribution of pollution exceedances.

Beyond the architecture, this paper contributes a formal mathematical treatment of the method: (i) it is proved that the quantile loss function recovers the conditional quantile, and its 19:1 gradient asymmetry at $\tau = 0.95$ is quantified; (ii) the "smoothing effect" of mean-optimal training is characterised through a peaks-over-threshold (POT) model, and it is proved that mean-trained detectors systematically miss an identifiable band of exceedances; and (iii) a decision-theoretic result (Theorem 1) is established, showing that thresholding a $\tau$-quantile forecast is Bayes-optimal for cost-sensitive exceedance alarms, with the optimal level fixed by the public-health cost ratio as $\tau^* = \mathrm{CFN}/(\mathrm{CFN}+\mathrm{CFP})$. This identity explains, rather than merely reports, the observed high-sensitivity, zero-false-alarm regime.

Hourly data from October 2022 to December 2023 were analysed, incorporating meteorological variables and co-pollutant concentrations as predictors. Statistical, machine learning, and deep learning models were compared. Deep learning consistently outperformed conventional approaches, capturing more than 70% of 24-hour and 60% of 48-hour extreme spikes at both stations. The proposed BEQ-GRU achieved the best performance for Colombo, while a standard Bidirectional GRU was most effective for Kandy. The framework can be adapted, with minor modifications, for proactive air-quality management and public-health early warning.

**Keywords:** PM2.5 forecasting; deep learning; Gated Recurrent Unit (GRU); quantile regression; extreme pollution events; decision theory; early-warning systems.

## 1 Introduction

Ambient fine particulate matter (PM2.5) poses a serious threat to human health and ecosystems. Owing to their small size ($\leq 2.5$ μm), PM2.5 particles penetrate deep into the lungs and bloodstream, contributing to respiratory and cardiovascular disease. Globally, exposure to PM2.5

is estimated to cause approximately 4.2 million premature deaths annually [1]. In response, the WHO updated its Global Air Quality Guidelines, recommending an annual mean PM2.5 limit of 5 µg/m3. These concerns have intensified interest in air-quality monitoring and forecasting.

In Sri Lanka, rapid urbanisation, vehicular traffic, and industrial activity have degraded air quality, particularly in Colombo, the capital city, and Kandy, which is situated in a low-lying valley surrounded by mountain ranges. The national annual average PM2.5 in 2022 was reported to be roughly 3.9 times the WHO guideline [2]. Major sources include vehicle exhaust, construction, and industrial emissions [3]. The associated health burden (asthma exacerbation, bronchitis, lung cancer, and cardiovascular disease) underscores the need for reliable short-term forecasting to support public-health protection [4].

Globally, advanced monitoring networks and predictive models, including machine-learning and deep-learning approaches, underpin operational early-warning systems. In contrast, forecasting capability in Sri Lanka remains limited: most local studies emphasise descriptive analysis of historical pollution rather than prediction [5], and few employ modern learning techniques under post-COVID emission and climatic conditions. Critically, no prior Sri Lankan study has explicitly targeted the forecasting of extreme PM2.5 occurrences, which carry the greatest health risk and most urgently require early warning.

Traditional models such as ARIMA capture trend and seasonality in univariate settings but underperform in multivariate systems and at longer horizons [12]. Machine-learning regressors (Random Forests, XGBoost) capture nonlinear relations [9] yet struggle with temporal dependence. Recurrent networks (LSTM and GRU) model sequential pollution data effectively [10], and bidirectional and attention-based variants further capture long-range dependencies [11]. Reviews of statistical and learning-based approaches to primary-pollutant forecasting survey this progression in detail [8], and recent work has applied LSTM and encoder-decoder architectures to air-quality index prediction [6,7]. However, a deeper methodological problem persists: the "smoothing effect" of central-tendency optimisation.

Standard networks minimise Mean Squared Error (MSE) or Mean Absolute Error (MAE), which target the conditional *mean* and *median* respectively. On heavy-tailed atmospheric data this optimisation under-represents extreme variance, smoothing high-magnitude spikes and causing systematic failure to detect hazardous exceedances [10,16]. The few studies that prioritise extremes (e.g. [13–15]) generally do not exploit deep learning to do so.

To address this gap, a shift from point-mean regression to risk-sensitive extremal forecasting is proposed. Quantile objectives have been combined with recurrent forecasters before, notably in the multi-horizon quantile recurrent forecaster of Wen et al. [17], which issues multi-step quantile predictions for demand series. To the best of current knowledge, however, this is the first study to integrate an asymmetric quantile objective ($\tau = 0.95$) within a bidirectional residual GRU specifically to capture the heavy-tailed distribution of PM2.5 exceedances, and the first to provide a decision-theoretic rule that fixes the quantile level from the public-health cost of a missed alarm. Concretely, the contributions are:

1. A novel architecture, BEQ-GRU, combining bidirectional encoding, residual GRU blocks, and an asymmetric quantile objective for multi-step PM2.5 forecasting at T+24 and T+48.

2. A complete mathematical formalisation of the model and a proof that the quantile loss function recovers the conditional 0.95-quantile, with an explicit characterisation of its gradient asymmetry.

**3.** A peaks-over-threshold justification of the smoothing effect and a proposition identifying the exact band of exceedances that mean-trained detectors miss but quantile detectors recover.

**4.** A decision-theoretic theorem proving that thresholding the τ-quantile forecast is Bayes-optimal for cost-sensitive exceedance alarms, fixing the optimal level as $\tau^* = C_{FN}/(C_{FN}+C_{FP})$; this explains the empirically observed zero-false-alarm, high-sensitivity regime. Here $C_{FN}$ is the cost of a false negative (a missed exceedance, i.e. failing to issue an alarm when PM2.5 exceeds the threshold) and $C_{FP}$ is the cost of a false positive (a false alarm issued when no exceedance occurs).

**5.** A comprehensive empirical comparison across statistical, machine-learning, and deep-learning models for Colombo and Kandy, with SHAP-based interpretation.

The next section of this article presents the methodology, and this section includes the mathematical justification of the proposed Bidirectional Enhanced Quantile GRU (BEQ-GRU) model. The final three sections provide results, discussion of the study followed by the conclusions.

# 2 Materials and Methods

## 2.1 Data Description

Two datasets were obtained from the Central Environmental Authority (CEA) of Sri Lanka, comprising hourly PM2.5 measurements from monitoring stations in Colombo and Kandy for the period from October 2022 to December 2023. PM2.5 is the target variable; predictors include ambient temperature, relative humidity, barometric pressure, solar radiation, rainfall, wind speed, wind direction, and concentrations of $O_3$, CO, $NO_2$, $NO_x$, $SO_2$, and PM10. Each dataset spans roughly 15 months (≈10,000 hourly observations per station after preprocessing).

## 2.2 Data Quality, Imputation, and Anomalies

Raw data contained missing values from sensor downtime and measurement anomalies. Variables with more than 60% missingness were excluded to avoid unreliable imputation [20], leaving 12 predictors for Colombo and 14 for Kandy. Two imputation strategies were evaluated: Bidirectional Recurrent Imputation for Time Series (BRITS) [18] and Self-Attention Imputation for Time Series (SAITS) [19]. SAITS consistently outperformed BRITS and interpolation and was selected, yielding continuous gap-free hourly series. Post-imputation, implausible negative readings were set to zero following CEA guidance; extreme PM2.5 peaks were retained as genuine pollution events to preserve the heavy-tailed structure central to this study.

## 2.3 Problem Formalisation

Let $x_t \in \mathbb{R}^p$ denote the multivariate observation at hour $t$, stacking the response (PM2.5) and $p-1$ predictors. For a current time $T$, the model consumes a look-back window of $L$ = 504 hours (21 days) and produces a forecast vector over horizon $H \in \{24, 48\}$:

$$X_T = (x_{T-L+1}, \dots, x_T) \in \mathbb{R}^{L \times p} \tag{1}$$

$$\hat{y}_T = f_\theta(X_T) \in \mathbb{R}^H, \quad y_T = (y_{T+1}, \dots, y_{T+H}) \tag{2}$$

Crucially, no future ground truth enters $X_T$; the map $f_\theta : \mathbb{R}^{L\times p} \to \mathbb{R}^H$ is learned at each station to capture location-specific dynamics. The remainder of Section 2 specifies the competing instantiations of $f_\theta$ and, for the proposed model, the objective that trains it.

## 2.4 Benchmark Models

### *2.4.1 Vector Autoregression (VAR)*

A VAR model was selected as the linear multivariate baseline, with PM2.5 as one endogenous variable alongside selected predictors. Stationarity was assessed via the Augmented Dickey–Fuller and seasonal unit-root tests [22]; non-stationary series were differenced and seasonally adjusted. Lag and predictor selection were based on Granger causality tests [21] and information criteria (Akaike Information Criterion, AIC, and Bayesian Information Criterion, BIC), with eigenvalue-based stability checks. Diagnostics covered residual autocorrelation (Ljung–Box), heteroscedasticity (White), and normality (Jarque–Bera). Forecasts were reconstructed on the original scale by additive decomposition: an extrapolated linear trend, an empirical hour-of-day seasonal profile, and VAR-forecasted residuals.

#### *2.4.2 Machine-Learning Models*

Random Forest (RF) and Extreme Gradient Boosting (XGBoost) [24] captured nonlinear relations. Unlike VAR, these tree-based models do not assume stationarity; they were trained directly on the raw (non-differenced) hourly series, with lagged values as features allowing them to capture trend and seasonality nonlinearly. A sliding-window transformation produced supervised samples using 504 hourly lags of all features, with outputs of the next 24 or 48 hourly PM2.5 values. Features were scaled with a robust (median/IQR) scaler; hyperparameters were tuned by grid search with cross-validation. Gini (RF) and gain (XGBoost) importance pruned the least informative predictors [23]; rainfall was consistently least informative and removed.

#### *2.4.3 Recurrent Deep-Learning Baselines and Advanced Variants*

Baseline LSTM and GRU networks used two stacked recurrent layers of 128 units, dropout (0.2), and a dense output layer, trained with Nadam, batch size 64, early stopping, and chronological 80/10/10 splits. Advanced variants added Bidirectional LSTM/GRU and multi-head-attention augmentation (four heads, residual connections). All used MAE or log-cosh losses for robustness to heavy-tailed residuals. These models motivate, but do not yet implement, an objective that targets the tail directly: the role of the proposed BEQ-GRU.

## 2.5 Proposed Bidirectional Enhanced Quantile GRU (BEQ-GRU)

The BEQ-GRU is designed around three requirements for extremal PM2.5 forecasting: (i) bidirectional temporal context to capture accumulation and dissipation phases of pollution episodes; (ii) gradient stability across a 504-step horizon via residual skip connections; and (iii) non-Gaussian error handling through an asymmetric quantile objective. Each component is specified as an explicit map.

### *2.5.1 GRU Cell*

Each recurrent unit updates its hidden state $h_t \in \mathbb{R}^d$ through an update gate $z_t$, a reset gate $r_t$, and a candidate state, where σ is the logistic sigmoid and ⊙ the Hadamard product [25]:

$$z_t = \sigma(W_z x_t + U_z h_{t-1} + b_z) \tag{3}$$

$$r_t = \sigma(W_r x_t + U_r h_{t-1} + b_r) \tag{4}$$

$$\hat{h}_t = tanh(W_h x_t + U_h(r_t \odot h_{t-1}) + b_h) \tag{5}$$

$$h_t = (1 - z_t) \odot h_{t-1} + z_t \odot \hat{h}_t \tag{6}$$

The gating preserves long-range information while remaining lighter than LSTM, reducing overfitting on the noisy environmental series. The parameters $W*$, $U*$, $b*$ with $* \in \{z, r, h\}$ in Eqs (3)-(5) are layer-specific.

### *2.5.2 Bidirectional Encoding*

Pollution occurrences evolve in both directions of accumulation and dissipation. The first layer therefore runs two GRUs over the window and concatenates their states [26]:

$$h_t^f = GRU^{fwd}(x_t, h_{t-1}^f), \quad h_t^b = GRU^{bwd}(x_t, h_{t+1}^b) \tag{7}$$

$$h_t = [h_t^f \oplus h_t^b] \in \mathbb{R}^{2d} \tag{8}$$

Concatenation (⊕) yields a representation conditioned on the full window, so that the model can anticipate a spike from its leading indicators as well as recognise its decay.

### *2.5.3 Residual GRU Blocks*

To stabilise gradients across the 504-step sequence, the encoder is stacked into $L_b$ residual blocks. For block $l$, with hidden sequence $\mathcal{H}(l-1) \in \mathbb{R}L\times2d$ from the previous block (script $\mathcal{H}$ denotes the hidden-sequence tensor, distinguishing it from the forecast horizon H), following the residual-connection and layer-normalisation formulation of He et al. and Ba et al. [27,28]:

$$g^{(l)} = BiGRU^{(l)}(\mathcal{H}^{(l-1)}) \tag{9}$$

$$\mathcal{H}^{(l)} = LayerNorm(W_p^{(l)}\mathcal{H}^{(l-1)} + g^{(l)}) \tag{10}$$

The projection $Wp(l) \in \mathbb{R}2d\times2d$ is applied time-distributed, i.e. broadcast identically across all L time steps, so that $Wp(l)\mathcal{H}(l-1) \in \mathbb{R}L\times2d$; it matches dimensions when they differ and is the identity otherwise. The additive skip connection guarantees an uninterrupted gradient path, mitigating vanishing gradients over three weeks of hourly data; layer normalisation stabilises the scale of the summed signal.

### *2.5.4 Output Head and Composition*

After $L_b$ blocks, the terminal hidden state $hT(Lb) \in \mathbb{R}2d$ is mapped linearly to the multi-step forecast by $Wo \in \mathbb{R}H\times2d$ and $bo \in \mathbb{R}H$:

$$\hat{y}_T = W_o h_T^{(L_b)} + b_o \in \mathbb{R}^H, \quad H \in \{24, 48\} \tag{11}$$

The full model is the composition $f_\theta$ = head ∘ (residual blocks) ∘ (bidirectional encoder), trained end-to-end under the objective of Section 2.6. Hyperparameters (number of blocks, hidden units, dropout, learning rate) were tuned with Keras Tuner on the validation set; the final configuration is in Table 1.

*Table 1. Architectural hyperparameters and configuration of the proposed BEQ-GRU.*

| Parameter | Configuration |
|---|---|
| Input window (look-back) | 504 hours (21 days) |
| Recurrent layers | Initial Bi-GRU (128 units) + multiple residual GRU blocks |
| Optimiser | Nadam |
| Loss function | Asymmetric quantile (check) loss, $\tau = 0.95$ |
| Regularisation | Dropout (0.2) and early stopping |
| Batch size | 64 |

## 2.6 The Asymmetric Quantile Objective

Standard losses estimate central tendency: MSE targets the conditional mean $E[Y|X]$ and MAE the conditional median. The BEQ-GRU instead targets the conditional 0.95-quantile $Q0.95[Y|X]$ via the quantile loss $\rho\tau$, the asymmetric piecewise-linear loss introduced by Koenker and Bassett [29]. For a residual $u = y - \hat{y}$ and level $\tau \in (0,1)$, $\rho\tau(u)$ denotes the loss incurred by that residual and is defined as:

$$\rho_\tau(u) = u(\tau - 1\{u < 0\}) = max\{\tau u, (\tau - 1)u\} \tag{12}$$

**Proposition 1 (Quantile consistency). Assume the conditional distribution function FY|X is continuous and strictly increasing in a neighbourhood of its τ-quantile, and that E|Y| < ∞. Then for any X, the minimiser** $q^* = \mathrm{argmin}_q\, E[\rho_\tau(Y - q) \mid X]$ satisfies $F_{Y|X}(q^*) = \tau$; that is, $q^* = Q_\tau(Y|X)$. The quantile loss function is therefore a consistent estimator of the conditional τ-quantile [29].

**Proof.** Let $g(q) = E[\rho_\tau(Y - q) \mid X]$. Writing $\rho_\tau$ as $\tau(Y-q)1\{Y\geq q\} + (\tau-1)(Y-q)1\{Y<q\}$ and differentiating under the integral (valid almost everywhere, a.e., since the integrand is piecewise linear with bounded slope, being non-differentiable only at the single point $q = Y$) gives:

$$g'(q) = -\tau\, P(Y > q \,|\, X) + (1-\tau)\, P(Y < q \,|\, X) = F_{Y|X}(q) - \tau \tag{13}$$

Since $g''(q) = f_{Y|X}(q) \geq 0$, g is convex, so the stationary point is the global minimiser. Setting $g'(q^*) = 0$ yields $F_{Y|X}(q^*) = \tau$, i.e. $q^* = Q_\tau(Y|X)$. ■

The sub-gradient of the loss with respect to the prediction makes the asymmetry explicit:

$$\frac{\partial \rho\tau}{\partial \hat{y}} = 1\{y < \hat{y}\} - \tau, \quad y \neq \hat{y} \tag{14}$$

At $\tau = 0.95$, under-forecasting ($y > \hat{y}$) incurs a gradient $-\tau = -0.95$, whereas over-forecasting ($y < \hat{y}$) incurs only $1 - \tau = 0.05$, a **19:1** penalty ratio against missing a peak. This is the mathematical mechanism that forces the network to track the upper tail rather than the centre of the distribution. The loss is not differentiable at $y = \hat{y}$, where the sub-differential is the interval $[-\tau, 1 - \tau]$; sub-gradient descent selects an element of this set, the standard treatment for piecewise-linear objectives. Over a training batch of $N$ samples and horizon $H$, training minimises the empirical loss $L(\theta)$, where $L$ denotes the quantile loss function (not a likelihood) and $\theta$ the network parameters:

$$L(\theta) = \frac{1}{NH}\sum_{i=1}^{N} \sum_{h=1}^{H} \rho_\tau(y_{i,h} - \hat{y}_{i,h}) \tag{15}$$

### 2.7 Extreme-Value Justification of the Smoothing Effect

The failure of mean-optimal training on exceedances is formalised using the peaks-over-threshold (POT) model. By the Pickands–Balkema–de Haan theorem [30–32], for a high threshold $u$, the conditional excess $Y - u \mid Y > u$ converges to a Generalised Pareto Distribution (GPD):

$$G_{\xi,\beta}(e) = 1 - (1 + \xi e/\beta)^{-1/\xi}, \quad e \geq 0,\ \xi \neq 0 \tag{16}$$

The tail index $\xi$ governs heaviness: $\xi > 0$ yields a heavy (fat) tail, exactly the regime of PM2.5 exceedances. The high quantile and the mean excess have closed forms,

$$Q_\alpha(Y) = u + \frac{\beta}{\xi}[\,((1-\alpha)/\zeta_u)^{-\xi} - 1\,], \quad E[Y - u \mid Y > u] = \frac{\beta}{1-\xi} \tag{17}$$

with $\zeta_u = P(Y > u)$. The mean excess is finite only for $\xi < 1$ and diverges as $\xi \to 1^-$, while quantiles remain finite throughout. The conditional mean is thus an unstable and downward-biased summary of the tail: the analytic root of the smoothing effect. The practical consequence is sharp:

**Proposition 2 (Missed-exceedance band).** Let $\mu(X) = E[Y|X]$ and let $F_{Y|X}$ be continuous and strictly increasing with positive skew so that $\mu(X) < Q_\tau(Y|X)$. For any regulatory threshold $c$ with $\mu(X) < c < Q_\tau(Y|X)$, a mean-optimal detector $\hat{y} = \mu(X)$ raises no alarm, even though $P(Y > c \mid X) > 1 - \tau > 0$, whereas the τ-quantile detector $\hat{y} = Q_\tau(Y|X) > c$ does. The mean detector therefore systematically misses every state in the band $(\mu(X), Q_\tau(Y|X))$ that the quantile detector recovers; this is the practical consequence of the fact that the optimal point forecast is determined by the loss functional used to elicit it [33].

### 2.8 Decision-Theoretic Selection of the Quantile Level (Principal Contribution)

Propositions 1–2 establish that a τ-quantile forecast detects more exceedances than a mean forecast, but the central operational question of which quantile level τ to use is left open. This question is addressed by casting the early-warning decision as cost-sensitive Bayesian classification and proving that the optimal level is fixed by the public-health cost ratio.

Let $c$ be the regulatory threshold (50 µg/m3 here), $e = 1\{Y > c\}$ the true exceedance, and $a \in \{0,1\}$ the alarm. Assign cost $C_{FN}$ to a missed exceedance ($a = 0$, e = 1), cost $C_{FP}$ to a false alarm ($a$ =1, $e$ = 0), and zero to correct decisions. Conditioning on $X$, the posterior expected costs of the two actions are:

$$E[cost \mid X, a = 1] = C_{FP} \cdot F_{Y|X}(c) \tag{18}$$

$$E[cost \mid X, a = 0] = C_{FN} \cdot (1 - F_{Y|X}(c)) \tag{19}$$

**Theorem 1 (Cost-optimal quantile level for exceedance alarms).** Under the loss above, and following the standard Bayes-risk minimisation argument for cost-sensitive decisions [34], the alarm minimising posterior expected cost is

$$a^*(X) = 1\{\, P(Y > c \mid X) > C_{FP}/(C_{FP} + C_{FN}) \,\} \tag{20}$$

Equivalently, defining $\tau^* = C_{FN}/(C_{FP} + C_{FN})$, this rule is identical to thresholding the $\tau^*$-quantile forecast at $c$:

$$a^*(X) = 1\{\, Q_{\tau^*}(Y \mid X) > c \,\}, \quad \tau^* = \frac{CFN}{CFP + CFN} \tag{21}$$

Hence, thresholding a calibrated $\tau^*$-quantile forecaster is Bayes-optimal for the early-warning decision, and the optimal quantile level is determined entirely by the cost ratio $\rho = C_{FP}/C_{FN}$, through $\tau^* = 1/(1 + \rho)$. The result assumes the cost ratio $\rho$ is fixed across the forecast horizon; where the consequences of a missed warning differ at 24 h and 48 h, $\tau^*$ should be set separately for each horizon.

**Proof.** Alarming is optimal iff (18) ≤ (19), i.e. $C_{FP}\cdot F_{Y|X}(c) \le C_{FN}\cdot(1-F_{Y|X}(c))$. Rearranging, $F_{Y|X}(c)\cdot(C_{FP}+C_{FN}) \le C_{FN}$, so $F_{Y|X}(c) \le C_{FN}/(C_{FP}+C_{FN}) = \tau^*$. Since F is non-decreasing, $F_{Y|X}(c) \le \tau^* \Leftrightarrow c \le Q_{\tau^*}(Y|X) \Leftrightarrow Q_{\tau^*}(Y|X) > c$ (taking the boundary into the alarm region). This is exactly Equation (21); and $P(Y>c|X) > C_{FP}/(C_{FP}+C_{FN})$ is the complementary form (20). ■

**Corollary 1 (Interpreting τ = 0.95).** Choosing $\tau = 0.95$ implies $\rho = (1-\tau)/\tau = 0.0526$, i.e. $C_{FN}/C_{FP} = 19$. BEQ-GRU's objective therefore encodes a policy in which a missed hazardous exceedance is treated as 19 times costlier than a false alarm, a defensible public-health stance and a precise, auditable statement of the model's risk preference.

**Remark.** Theorem 1 explains the empirical results of Section 3. $\tau^* = 0.95$ places the implicit decision boundary high in the conditional distribution, false alarms become rare (consistent with the observed zero false positives) while sensitivity to genuine exceedances stays high. The architecture and the objective are thus not independent design choices: the quantile level is the tuning knob that translates a stated cost ratio into the detector's operating point. To the best of current knowledge, this explicit link (selecting τ from the missed-alarm cost for PM2.5 early warning) has not previously been used in air-quality forecasting.

## 2.9 Evaluation Metrics

Point accuracy is assessed by Root Mean Squared Error (RMSE), Mean Absolute Error (MAE), and Mean Absolute Percentage Error (MAPE):

$$RMSE = \sqrt{\frac{1}{n}\sum_{i=1}^{n}(y_{\mathrm{i}} - \hat{y}_{\mathrm{i}})^2} \quad (22)$$

$$MAE = \frac{1}{n}\sum_{i=1}^{n}|y_{\mathrm{i}} - \hat{y}_{\mathrm{i}}|, \quad MAPE = \frac{1}{n}\sum_{i=1}^{n}|(y_{\mathrm{i}} - \hat{y}_{\mathrm{i}})/y_{\mathrm{i}}| \quad (23)$$

Public-health relevance is assessed by exceedance detection at $c$ = 50 μg/m3 [35]. From the confusion matrix of true/false positives and negatives,

$$Detection\ Rate\ (Sensitivity) = \frac{TP}{TP + FN}, \quad Precision = \frac{TP}{TP + FP} \quad (24)$$

Sensitivity is the operationally decisive metric for early warning, since a missed exceedance carries the cost $C_{FN}$ of Theorem 1.

## 2.10 Statistical analysis

All analyses were carried out in Python 3.11.9. Deep-learning models were implemented in TensorFlow 2.16.1 with Keras 3.3.3 and hyperparameters selected using Keras Tuner 1.4.7; tree-based models used scikit-learn 1.5.2 and XGBoost 2.1.1; vector autoregression, unit-root testing and diagnostics used statsmodels 0.14.4; and SHAP values were computed with the shap package 0.46.0.

Hypothesis tests, including the Augmented Dickey-Fuller and KPSS unit-root tests, the Granger causality tests used for predictor selection, and the Ljung-Box, White and Jarque-Bera residual diagnostics, were evaluated at a significance level of alpha = 0.05; exact p-values are reported in S2 Table.

Missing observations, which affected a substantial fraction of the record at both stations, were imputed with SAITS as described in Section 2.2; no observations were deleted on the basis of missingness. Extreme values were retained rather than winsorised, since exceedances are the target of the analysis; consequently, no outlier-removal step was applied and no sensitivity analysis excluding outliers is reported. Predictors were scaled with a median/interquartile-range robust scaler fitted on the training partition only, so that no validation or test information entered the scaling.

Data were split chronologically into training, validation and test partitions in an 80/10/10 ratio, with no shuffling, so that all evaluation is out-of-sample and forward in time. Point accuracy is reported as RMSE, MAE and MAPE, and exceedance performance as detection rate (sensitivity) and precision against the 50 μg/m3 threshold, with the counts behind every rate given in the corresponding table.

# 3 Results

## 3.1 Data Overview and Exploratory Findings

Fig 1 shows daily average PM2.5 at both cities from October 2022 to December 2023. Colombo exhibits sustained elevated levels from November to January, coinciding with the Northeast monsoon and stagnant conditions; Kandy's peaks are more episodic, with an isolated extreme spike in early 2023.

*Figure 1. Daily average PM2.5 concentration, October 2022 to December 2023. (A) Colombo. (B) Kandy.*

Using a chronological 80/10/10 split, extreme events (>50 µg/m3) are consistently distributed across subsets (Table 2). Colombo shows a higher overall frequency (≈3.6%) than Kandy (≈2.5%), motivating the station-specific, extreme-focused architecture.

*Table 2. Distribution of PM2.5 extreme events across data splits.*

| Station | Split | Total hours | Extreme events (>50) | Extreme (%) |
|---|---|---|---|---|
| Colombo | Training (80%) | 8,776 | 312 | 3.56% |
| Colombo | Validation (10%) | 1,096 | 39 | 3.56% |
| Colombo | Testing (10%) | 1,096 | 41 | 3.74% |
| Kandy | Training (80%) | 8,776 | 234 | 2.67% |
| Kandy | Validation (10%) | 1,096 | 26 | 2.37% |
| Kandy | Testing (10%) | 1,096 | 28 | 2.55% |

## 3.2 Traditional Statistical Model (VAR)

Stationarity was confirmed via the Augmented Dickey–Fuller and seasonal unit-root tests described in Section 2.4.1; the resulting detrending and deseasonalisation ensured stationarity, but cointegration tests found no stable long-run relationships, and residuals showed heteroscedasticity and non-normality (relaxed for forecasting) [36]. The VAR produced relatively high errors (Table 3, Fig 2), confirming the limited ability of linear models to capture nonlinear, highly variable pollution dynamics.

*Table 3. VAR model performance.*

| Error measure | Colombo 24 h | Colombo 48 h | Kandy 24 h | Kandy 48 h |
|---|---|---|---|---|
| **RMSE** | 11.20 | 11.32 | 5.10 | 5.31 |
| **MAE** | 9.36 | 9.39 | 4.20 | 4.81 |
| **MAPE** | 0.83 | 0.93 | 0.89 | 0.95 |

**Fig 2.** Observed and forecast PM2.5 concentration from the VAR model. (A) Colombo. (B) Kandy.

The 48-hour VAR forecast (red) visibly lags and smooths the actual series (blue) at both stations: it fails to track the sharp peaks near t≈10927 (Colombo) and t≈10951 (Kandy), instead tracing a damped, delayed version of the true trajectory. This is a direct visual instance of the meanreversion behaviour formalised in Proposition 2 and Section 2.7: the linear model's forecasts regress toward the conditional mean and systematically under-predict exceedances.

### 3.3 Machine-Learning Models

After removing the least informative predictor (rainfall), Random Forest and XGBoost were trained on raw, non-differenced series since tree-based models do not require stationarity (refer to Section 2.4.2); both improved over VAR (Tables 4–5). For Colombo, RF reached a 24-hour RMSE of 10.74 µg/m3; for Kandy, XGBoost edged ahead at 4.37 µg/m3. Despite lower average errors, both struggled with extremes: RF captured under 10% of Colombo's 24-hour exceedances and none at 48 hours; XGBoost reached roughly 61% (24 h) and 29% (48 h) at Colombo and 65%/55% at Kandy, a direct empirical instance of Proposition 2.

*Table 4. Optimised Random Forest performance.*

| Error measure | Colombo 24 h | Colombo 48 h | Kandy 24 h | Kandy 48 h |
|---|---|---|---|---|
| **RMSE (µg/m3)** | 10.74 | 12.03 | 4.49 | 5.03 |
| **MAE (µg/m3)** | 7.80 | 8.69 | 3.61 | 3.99 |
| **MAPE** | 0.76 | 0.89 | 0.85 | 0.91 |

*Table 5. Optimised XGBoost performance.*

| Error measure | Colombo 24 h | Colombo 48 h | Kandy 24 h | Kandy 48 h |
|---|---|---|---|---|
| **RMSE (µg/m3)** | 11.75 | 13.72 | 4.37 | 5.06 |
| **MAE (µg/m3)** | 8.48 | 9.92 | 3.38 | 3.96 |
| **MAPE** | 0.75 | 0.85 | 0.82 | 0.89 |

### 3.4 Deep-Learning Models

Baseline LSTM and GRU improved on the machine-learning regressors (Table 6). GRU marginally outperformed LSTM in both cities and horizons, likely owing to its simpler gating and lower overfitting risk; for Colombo it reached a 24-hour RMSE of 10.59 µg/m3, and for Kandy 3.99 µg/m3. Still, baseline RNNs remained limited on extreme spikes.

*Table 6. Baseline LSTM and GRU performance.*

| Model and station | RMSE 24 h | RMSE 48 h | MAE 24 h | MAE 48 h | MAPE 24 h | MAPE 48 h |
|---|---|---|---|---|---|---|
| **LSTM (Colombo)** | 10.77 | 11.76 | 8.03 | 8.47 | 0.72 | 0.81 |
| **GRU (Colombo)** | 10.59 | 11.33 | 7.87 | 8.28 | 0.69 | 0.78 |
| **LSTM (Kandy)** | 4.43 | 4.94 | 3.57 | 3.86 | 0.78 | 0.85 |
| **GRU (Kandy)** | 3.99 | 4.81 | 3.17 | 3.74 | 0.75 | 0.81 |

Among advanced architectures (Table 7), the Bi-GRU was strongest overall: for Colombo it cut the 24-hour MAPE to 0.52 and RMSE to 10.49 µg/m3; for Kandy it achieved the lowest RMSE (3.89) and MAPE (0.56). Multi-head attention did not yield consistent gains, suggesting recurrent layers alone captured the dominant dependencies. Errors were uniformly lower at Kandy, reflecting its lower levels and fewer extremes, leaving Colombo's frequent exceedances as the motivation for the BEQ-GRU.

*Table 7. Advanced (bidirectional and attention-based) model performance.*

| Model and station | RMSE 24 h | RMSE 48 h | MAE 24 h | MAE 48 h | MAPE 24 h | MAPE 48 h |
|---|---|---|---|---|---|---|
| **Bi-LSTM (Colombo)** | 10.13 | 11.84 | 7.51 | 8.63 | 0.58 | 0.66 |
| **Bi-GRU (Colombo)** | 10.49 | 11.29 | 7.69 | 8.13 | 0.52 | 0.59 |
| **Bi-LSTM (Kandy)** | 4.12 | 4.56 | 3.25 | 3.56 | 0.61 | 0.73 |
| **Bi-GRU (Kandy)** | 3.89 | 4.44 | 3.07 | 3.41 | 0.56 | 0.71 |
| **MHA+Bi-LSTM (Col)** | 10.87 | 12.17 | 8.04 | 8.92 | 0.67 | 0.75 |
| **MHA+Bi-LSTM (Kan)** | 5.04 | 5.78 | 4.07 | 4.59 | 0.65 | 0.77 |
| **MHA+Bi-GRU (Col)** | 10.44 | 11.65 | 7.85 | 8.95 | 0.63 | 0.70 |
| **MHA+Bi-GRU (Kan)** | 4.68 | 5.19 | 3.73 | 4.11 | 0.63 | 0.75 |

## 3.5 Proposed BEQ-GRU

For Colombo, the BEQ-GRU achieved the best overall accuracy (24-hour RMSE 9.88 µg/m3, MAPE 0.48), surpassing the next-best Bi-GRU and Bi-LSTM at both horizons (Table 8). For Kandy, the standard Bi-GRU remained superior, consistent with its lower exceedance frequency and the suitability of mean-error training there, precisely the regime where Corollary 1's 19:1 cost preference offers little marginal benefit.

*Table 8. Best models per station: BEQ-GRU (Colombo) and Bi-GRU (Kandy).*

| Station (model) | RMSE 24 h | RMSE 48 h | MAE 24 h | MAE 48 h | MAPE 24 h | MAPE 48 h |
|---|---|---|---|---|---|---|
| **Colombo (BEQ-GRU)** | 9.88 | 11.13 | 7.38 | 8.02 | 0.48 | 0.55 |
| **Kandy (Bi-GRU)** | 4.11 | 4.51 | 3.22 | 3.60 | 0.59 | 0.73 |

The decisive comparison is extreme-event detection (Table 9). While Simple GRU and XGBoost detect reasonably at 24 hours, their sensitivity collapses at 48 hours. The BEQ-GRU (Colombo, 41 extreme events) and Bi-GRU (Kandy, 28 extreme events) sustain the highest sensitivity across both horizons, and, as Theorem 1 predicts for a high τ*, produce zero false positives.

*Table 9. Extreme PM2.5 event detection (>50 µg/m3) across main models.*

| Station | Model | Horizon | TP | FN | Detection (%) |
|---|---|---|---|---|---|
| **Colombo (41)** | BEQ-GRU | 24 h | 30 | 11 | 73.17% |
| **Colombo (41)** | BEQ-GRU | 48 h | 25 | 16 | 60.97% |
| **Colombo (41)** | Simple GRU | 24 h | 25 | 16 | 60.98% |
| **Colombo (41)** | Simple GRU | 48 h | 14 | 27 | 34.15% |
| **Colombo (41)** | XGBoost | 24 h | 25 | 16 | 60.94% |
| **Colombo (41)** | XGBoost | 48 h | 12 | 29 | 29.33% |
| **Colombo (41)** | Random Forest | 24 h | 4 | 37 | 9.52% |
| **Colombo (41)** | Random Forest | 48 h | 0 | 41 | 0.00% |
| **Kandy (28)** | Bi-GRU | 24 h | 20 | 8 | 71.43% |
| **Kandy (28)** | Bi-GRU | 48 h | 17 | 11 | 60.71% |
| **Kandy (28)** | Simple GRU | 24 h | 17 | 11 | 60.71% |
| **Kandy (28)** | XGBoost | 24 h | 18 | 10 | 65.35% |
| **Kandy (28)** | Random Forest | 24 h | 15 | 13 | 54.93% |

Confusion matrices for the top models (Tables 10–11) confirm zero false positives at both horizons, i.e. improved sensitivity without additional false alarms.

*Table 10. Confusion matrix, BEQ-GRU (Colombo).*

| Actual \ Forecast | 24 h BT | 24 h OT | 48 h BT | 48 h OT |
|---|---|---|---|---|
| **Below threshold (BT)** | 1015 | 0 | 1015 | 0 |
| **Over threshold (OT)** | 11 | 30 | 16 | 25 |

*Table 11. Confusion matrix, Bi-GRU (Kandy).*

| Actual \ Forecast | 24 h BT | 24 h OT | 48 h BT | 48 h OT |
|---|---|---|---|---|
| **Below threshold (BT)** | 1028 | 0 | 1028 | 0 |
| **Over threshold (OT)** | 8 | 20 | 11 | 17 |

**Fig 3.** Observed and forecast PM2.5 concentration for Colombo from the BEQ-GRU. (A) 24 h ahead. (B) 48 h ahead. The dashed line marks the 50 μg/m3 regulatory threshold.

**Fig 4.** Observed and forecast PM2.5 concentration for Kandy from the bidirectional GRU. (A) 24 h ahead. (B) 48 h ahead.

Across both stations, the deep-learning forecasts track exceedance timing far better than the VAR baseline in Fig 2. The Colombo BEQ-GRU (Fig 3) follows the sharp upward excursions above the 50 μg/m3 threshold (dashed line) at both horizons, correctly flagging most crossings without triggering a false alarm when the actual series stays below the line; the 48-hour panel shows some flattening of peak magnitude relative to 24 hours, consistent with the lower 48-hour detection rate in Table 9 (60.97% versus 73.17%). The Kandy Bi-GRU (Fig 4) shows the same pattern at a lower exceedance frequency: it tracks the actual series closely at 24 hours (71.43% detection, Table 9) with some peak attenuation at 48 hours (60.71% detection), and the confusion matrix in Table 11 confirms zero false positives at either horizon. In both cases, the model tracks the timing of exceedance onsets rather than reverting to the mean the way VAR does.

### 3.6 Explainability (SHAP)

SHAP [37,38] analysis via the Gradient Explainer interprets the best models at both horizons. Across stations, past PM2.5 was the dominant predictor of future values. Co-pollutants (especially PM10 and $NO_2$) outranked meteorological variables: at Kandy, PM10 and $NO_2$ were the top contributors; at Colombo, PM10 and NO also showed strong influence, reinforcing the role of pollutant interdependence in near-term air quality.

**Fig 5.** SHAP feature importance for Colombo. (A) 24 h ahead. (B) 48 h ahead.

**Fig 6.** SHAP feature importance for Kandy. (A) 24 h ahead. (B) 48 h ahead.

# 4 Discussion

The advanced deep-learning models (BEQ-GRU and Bi-GRU) delivered strong overall accuracy and, more importantly, the ability to forecast extreme episodes. Relative to ARIMA-type methods [12], they integrate multivariate meteorological and pollutant inputs and handle the nonlinear, stochastic behaviour of tropical atmospheric chemistry without Gaussian assumptions.

A unifying explanation runs through the paper's theory (Propositions 1–2, Section 2.7; Theorem 1 and Corollary 1, Section 2.8). Most standard regressors are conditional-mean estimators; by Proposition 2, they sit below the regulatory threshold for an identifiable band of states and miss those exceedances. The BEQ-GRU instead estimates the conditional 0.95-quantile (Proposition 1), and by Theorem 1, thresholding that quantile is the Bayes-optimal alarm under a 19:1 missed-to-false-alarm cost (Corollary 1). The smoothing failure of RF and XGBoost on Colombo's extremes, and the high-sensitivity / zero-false-alarm behaviour of the quantile models, are therefore predicted, not merely observed.

Feature importance was informative: past PM2.5 was the most influential predictor (consistent with [5,39]), followed by PM10, $NO_2$, and CO, with meteorology secondary. Wrapper-style pruning reduced dimensionality and overfitting [40]. Unlike many global studies where meteorology dominates, pollutant interdependence drove short-term PM2.5 here, suggesting that investment in co-pollutant sensors may yield greater short-range forecasting benefit than complex meteorological modelling in similar tropical monsoon climates.

Methodologically, the principal contribution is the explicit bridge between the training objective and the operational decision: the quantile level $\tau$ is not a hyperparameter to be tuned blindly but a policy parameter set by the cost of a missed warning. This reframes extreme-event forecasting as risk-sensitive decision-making and offers a transferable recipe for other hazards with asymmetric consequences.

## 5 Conclusion

Deep-learning models outperformed both statistical (VAR) and machine-learning (RF, XGBoost) approaches for short-term PM2.5 forecasting in Sri Lanka. The proposed BEQ-GRU was best for Colombo's frequent, intense extremes, while the standard Bi-GRU sufficed for Kandy's sparser events. Beyond empirical gains, the paper supplies a mathematical foundation: a consistency proof for the quantile objective, an extreme-value account of the smoothing effect, and a decision-theoretic theorem fixing the optimal quantile level from the public-health cost ratio. SHAP analysis identified past PM2.5, PM10, and gaseous pollutants as the dominant drivers. Together, these results support operational, risk-sensitive early-warning systems for hazardous pollution.

## 6 Limitations and Future Work

The ≈15-month record limits learning of interannual variability, and substantial missingness introduced uncertainty despite deep-learning imputation. Spatial coverage was confined to Colombo and Kandy, constraining generalisation. Future work should extend the temporal range; add predictors such as traffic intensity, industrial activity, and monsoon dynamics; incorporate transboundary pollution (notably from southern India); and estimate the cost ratio $\rho$ empirically so that $\tau^*$ can be calibrated to local health-economic data rather than fixed a priori.

## Acknowledgments

The authors thank the Central Environmental Authority of Sri Lanka for providing the air-quality and meteorological monitoring data used in this study, and the Department of Statistics, University of Colombo, for computational support.

## References

1. World Health Organization. Ambient (outdoor) air pollution. Geneva: World Health Organization; 2024 [cited 2026 Aug 23]. Available from: https://www.who.int/news-room/fact-sheets/detail/ambient-(outdoor)-air-quality-and-health

2. Senarathna M, Weerasundara L, Magana-Arachchi D, Nanayakkara N, Wanigasuriya K. PM2.5 air pollution trends and patterns in Kandy, Sri Lanka. Ceylon J Sci. 2024;53: 197-206.

3. Ileperuma OA. Review of air pollution studies in Sri Lanka. Ceylon J Sci. 2020;49: 225-238.

4. Xing YF, Xu YH, Shi MH, Lian YX. The impact of PM2.5 on the human respiratory system. J Thorac Dis. 2016;8: E69-E74. doi: 10.3978/j.issn.2072-1439.2016.01.19

5. Mampitiya L, Rathnayake N, Leon LP, Mandala V, Azamathulla HM, Shelton S, et al. Machine learning techniques to predict the air quality using meteorological data in two urban areas in Sri Lanka. Environments. 2023;10: 141. doi: 10.3390/environments10080141

6. Drewil GI, Al-Bahadili RJ. Air pollution prediction using LSTM deep learning and metaheuristics algorithms. Meas Sens. 2022;24: 100546. doi: 10.1016/j.measen.2022.100546

7. Feng H, Zhang X. A novel encoder-decoder model based on Autoformer for air quality index prediction. PLoS One. 2023;18: e0284293. doi: 10.1371/journal.pone.0284293

8. Liao K, Huang X, Dang H, Ren Y, Zuo S, Duan C. Statistical approaches for forecasting primary air pollutants: a review. Atmosphere. 2021;12: 686. doi: 10.3390/atmos12060686

9. Ravindiran G, Hayder G, Kanagarathinam K, Alagumalai A, Sonne C. Air quality prediction by machine learning models: a predictive study on the Indian coastal city of Visakhapatnam. Chemosphere. 2023;338: 139518. doi: 10.1016/j.chemosphere.2023.139518

10. Zhang Z, Zhang S, Chen C, Yuan J. A systematic survey of air quality prediction based on deep learning. Alex Eng J. 2024;93: 128-141. doi: 10.1016/j.aej.2024.03.031

11. Zhang Y, Sun Q, Liu J, Petrosian O. Long-term forecasting of air pollution PM2.5 and analysis of influencing factors. Sustainability. 2023;16: 19. doi: 10.3390/su16010019

12. Marinov E, Petrova-Antonova D, Malinov S. Time series forecasting of air quality: a case study of Sofia city. Atmosphere. 2022;13: 788. doi: 10.3390/atmos13050788

13. Zhou SM, Deng QH, Liu WW. Extreme air pollution events: modeling and prediction. J Cent South Univ. 2012;19: 1668-1672. doi: 10.1007/s11771-012-1191-2

14. Barthwal A, Acharya D, Lohani D. IoT system based forecasting and modeling exceedance probability and return period of air quality using extreme value distribution. In: Proceedings of the 2019 IEEE Sensors Applications Symposium (SAS); 2019 Mar 11-13; Sophia Antipolis, France. Piscataway (NJ): IEEE; 2019. pp. 1-6.

15. Gul S, Khan GM. Forecasting hazard level of air pollutants using LSTM. In: Maglogiannis I, Iliadis L, Pimenidis E, editors. Artificial Intelligence Applications and Innovations (AIAI 2020). IFIP Advances in Information and Communication Technology, vol 584. Cham: Springer; 2020. pp. 143-153.

16. Mienye ID, Swart TG. A comprehensive review of deep learning: architectures, recent advances, and applications. Information. 2024;15: 755. doi: 10.3390/info15120755

17. Wen R, Torkkola K, Narayanaswamy B, Madeka D. A multi-horizon quantile recurrent forecaster. arXiv:1711.11053 [Preprint]. 2017 [cited 2026 Aug 23]. Available from: https://arxiv.org/abs/1711.11053

18. Cao W, Wang D, Li J, Zhou H, Li Y, Li L. BRITS: bidirectional recurrent imputation for time series. In: Advances in Neural Information Processing Systems 31 (NeurIPS 2018); 2018 Dec 3-8; Montreal, Canada. Red Hook (NY): Curran Associates; 2018. pp. 6775-6785.

19. Du W, Cote D, Liu Y. SAITS: self-attention-based imputation for time series. Expert Syst Appl. 2023;219: 119619. doi: 10.1016/j.eswa.2023.119619

20. Le LP, Nguyen TH, Tran MQ, Pham DT, Vo HT, Dang NM, et al. Missing data imputation for noisy time-series data and applications in healthcare. arXiv:2412.11164 [Preprint]. 2024 [cited 2026 Aug 23]. Available from: https://arxiv.org/abs/2412.11164

21. Granger CWJ. Investigating causal relations by econometric models and cross-spectral methods. Econometrica. 1969;37: 424-438. doi: 10.2307/1912791

22. Heaps SE. Enforcing stationarity through the prior in vector autoregressions. J Comput Graph Stat. 2023;32: 74-83. doi: 10.1080/10618600.2022.2079648

23. Kathirgamanathan B, Cunningham P. A feature selection method for multi-dimension time-series data. In: Lemaire V, Malinowski S, Bagnall A, Guyet T, Tavenard R, Ifrim G, editors. Advanced Analytics and Learning on Temporal Data (AALTD 2020). Lecture Notes in Computer Science, vol 12588. Cham: Springer; 2020. pp. 220-231.

24. Breiman L. Random forests. Mach Learn. 2001;45: 5-32. doi: 10.1023/A:1010933404324

25. Cho K, van Merrienboer B, Gulcehre C, Bahdanau D, Bougares F, Schwenk H, et al. Learning phrase representations using RNN encoder-decoder for statistical machine translation. In: Proceedings of the 2014 Conference on Empirical Methods in Natural Language Processing (EMNLP); 2014 Oct 25-29; Doha, Qatar. Stroudsburg (PA): Association for Computational Linguistics; 2014. pp. 1724-1734. doi: 10.3115/v1/D14-1179

26. Schuster M, Paliwal KK. Bidirectional recurrent neural networks. IEEE Trans Signal Process. 1997;45: 2673-2681. doi: 10.1109/78.650093

27. He K, Zhang X, Ren S, Sun J. Deep residual learning for image recognition. In: Proceedings of the 2016 IEEE Conference on Computer Vision and Pattern Recognition (CVPR); 2016 Jun 27-30; Las Vegas, NV, USA. Piscataway (NJ): IEEE; 2016. pp. 770-778. doi: 10.1109/CVPR.2016.90

28. Ba JL, Kiros JR, Hinton GE. Layer normalization. arXiv:1607.06450 [Preprint]. 2016 [cited 2026 Aug 23]. Available from: https://arxiv.org/abs/1607.06450

29. Koenker R, Bassett G. Regression quantiles. Econometrica. 1978;46: 33-50. doi: 10.2307/1913643

30. Balkema AA, de Haan L. Residual life time at great age. Ann Probab. 1974;2: 792-804. doi: 10.1214/aop/1176996548

31. Pickands J. Statistical inference using extreme order statistics. Ann Stat. 1975;3: 119-131. doi: 10.1214/aos/1176343003

32. Coles S. An introduction to statistical modeling of extreme values. London: Springer; 2001.

33. Gneiting T. Making and evaluating point forecasts. J Am Stat Assoc. 2011;106: 746-762. doi: 10.1198/jasa.2011.r10138

34. Elkan C. The foundations of cost-sensitive learning. In: Proceedings of the 17th International Joint Conference on Artificial Intelligence (IJCAI); 2001 Aug 4-10; Seattle, WA, USA. San Francisco (CA): Morgan Kaufmann; 2001. pp. 973-978.

35. Government of Sri Lanka. The Gazette of the Democratic Socialist Republic of Sri Lanka, Part I, Section (I). Colombo: Department of Government Printing; 2008.

36. Lutkepohl H. New introduction to multiple time series analysis. Berlin: Springer; 2005.

37. Lundberg SM, Lee SI. A unified approach to interpreting model predictions. In: Advances in Neural Information Processing Systems 30 (NIPS 2017); 2017 Dec 4-9; Long Beach, CA, USA. Red Hook (NY): Curran Associates; 2017. pp. 4765-4774.

38. Shapley LS. A value for n-person games. In: Kuhn HW, Tucker AW, editors. Contributions to the theory of games, volume II. Annals of Mathematics Studies, vol 28. Princeton (NJ): Princeton University Press; 1953. pp. 307-317.

39. Mohan AS, Abraham L. An ensemble deep learning model for forecasting hourly PM2.5 concentrations. IETE J Res. 2023;69: 6832-6845. doi: 10.1080/03772063.2021.1963332

40. Farheen, Kumar R. Composition of feature selection for time-series prediction with deep learning. Procedia Comput Sci. 2024;235: 1477-1488. doi: 10.1016/j.procs.2024.04.139

(A)

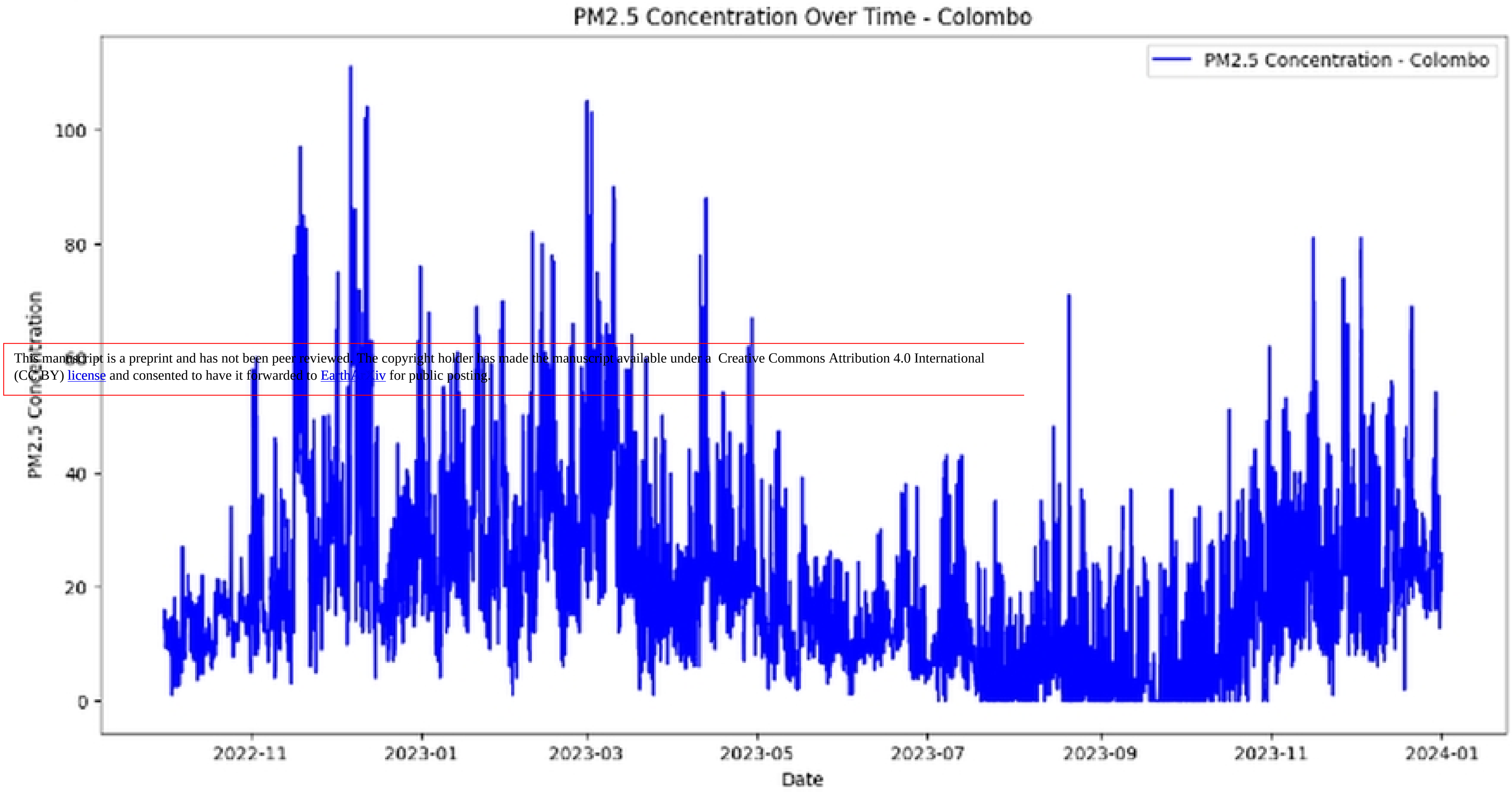
PM2.5 Concentration Over Time - Colombo
PM2.5 Concentration - Colombo
PM2.5 Concentration
0
20
40
60
80
100
2022-11
2023-01
2023-03
2023-05
2023-07
2023-09
2023-11
2024-01
Date



(B)

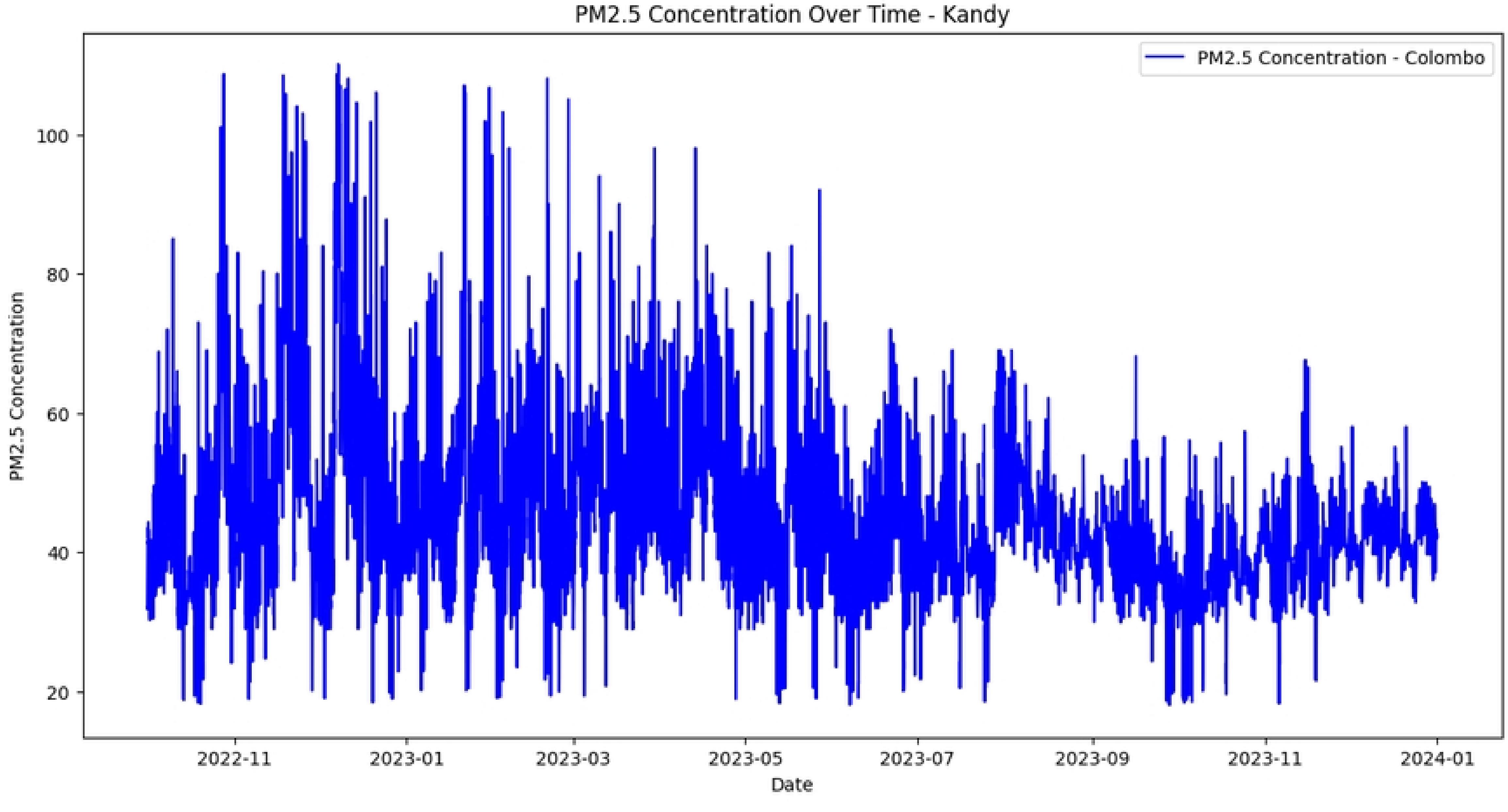
PM2.5 Concentration Over Time - Kandy
PM2.5 Concentration - Colombo
PM2.5 Concentration
20
40
60
80
100
2022-11
2023-01
2023-03
2023-05
2023-07
2023-09
2023-11
2024-01
Date

(A)

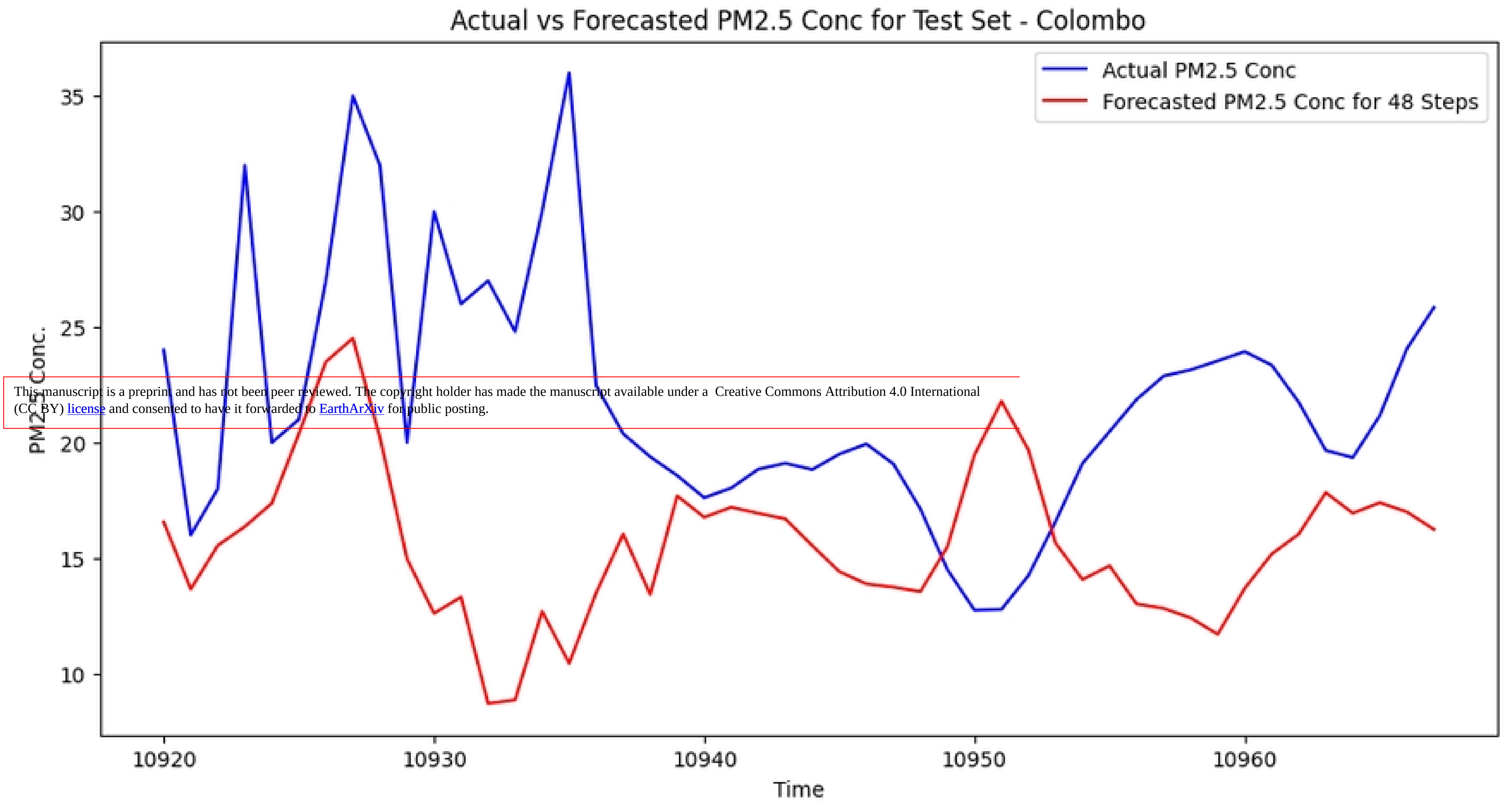
Actual vs Forecasted PM2.5 Conc for Test Set - Colombo
Actual PM2.5 Conc
Forecasted PM2.5 Conc for 48 Steps
PM2.5 Conc.
Time



(B)

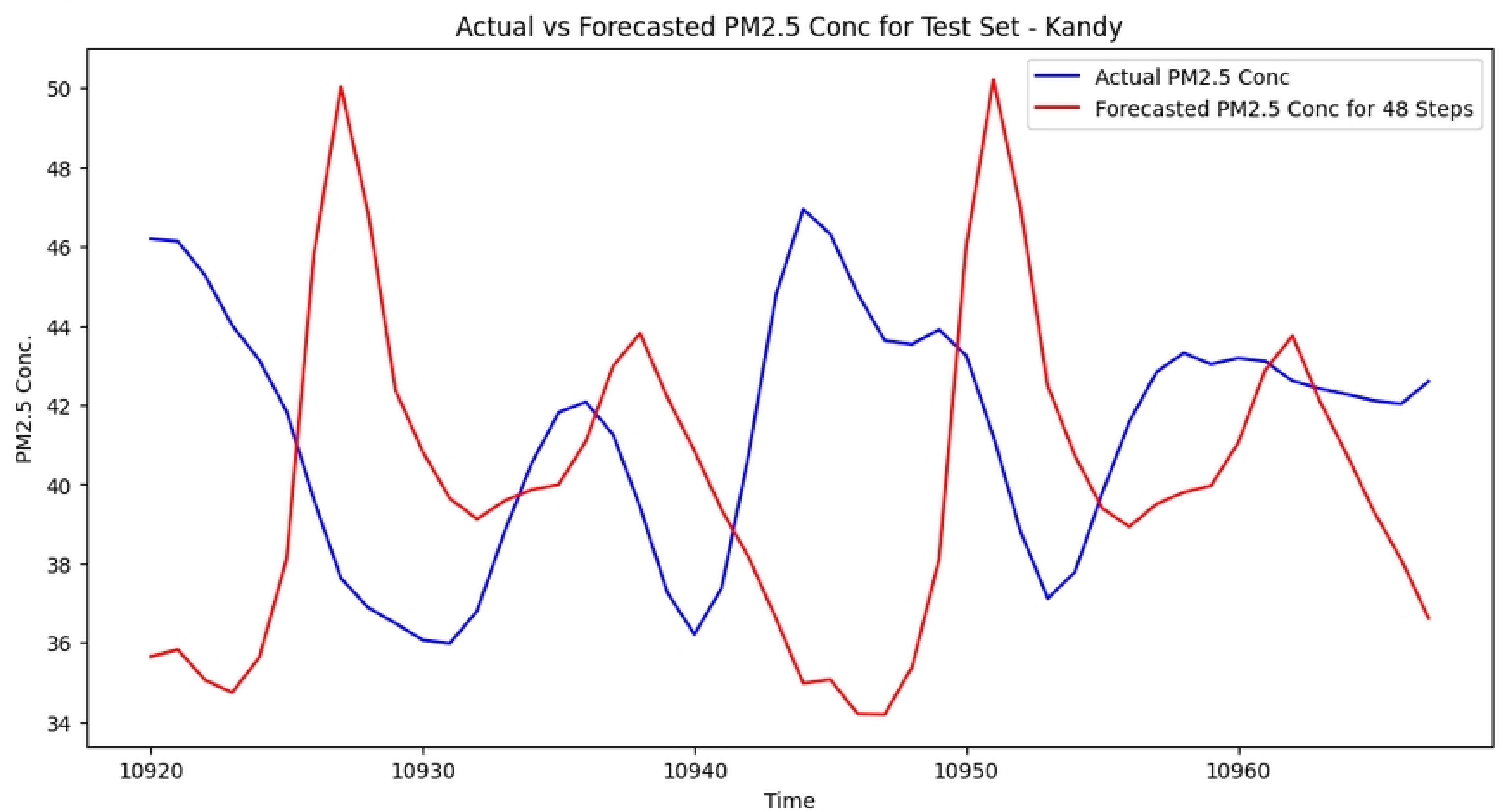
Actual vs Forecasted PM2.5 Conc for Test Set - Kandy
Actual PM2.5 Conc
Forecasted PM2.5 Conc for 48 Steps
PM2.5 Conc.
Time

**(A)**

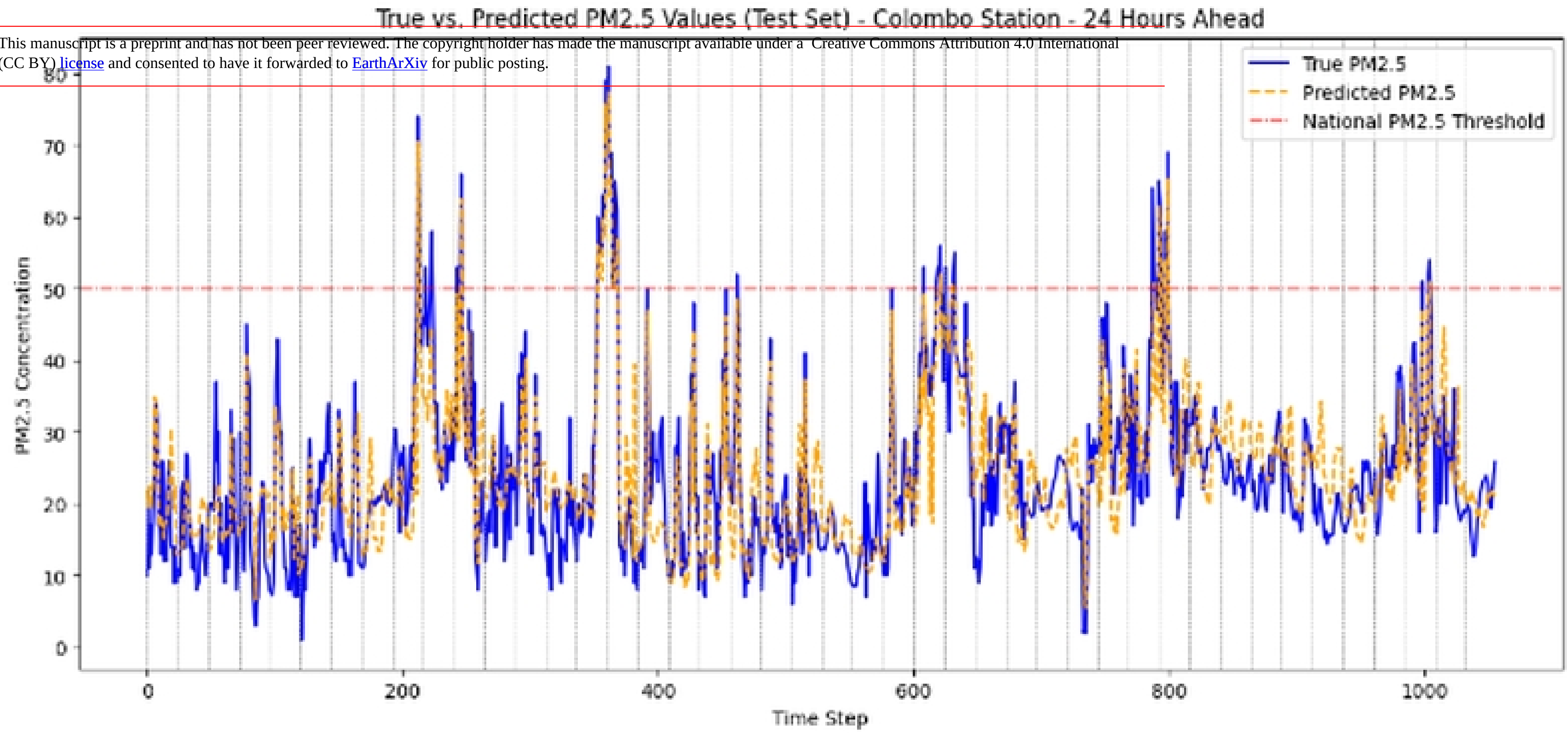
True vs. Predicted PM2.5 Values (Test Set) - Colombo Station - 24 Hours Ahead
True PM2.5
Predicted PM2.5
National PM2.5 Threshold
PM2.5 Concentration
Time Step

**(B)**

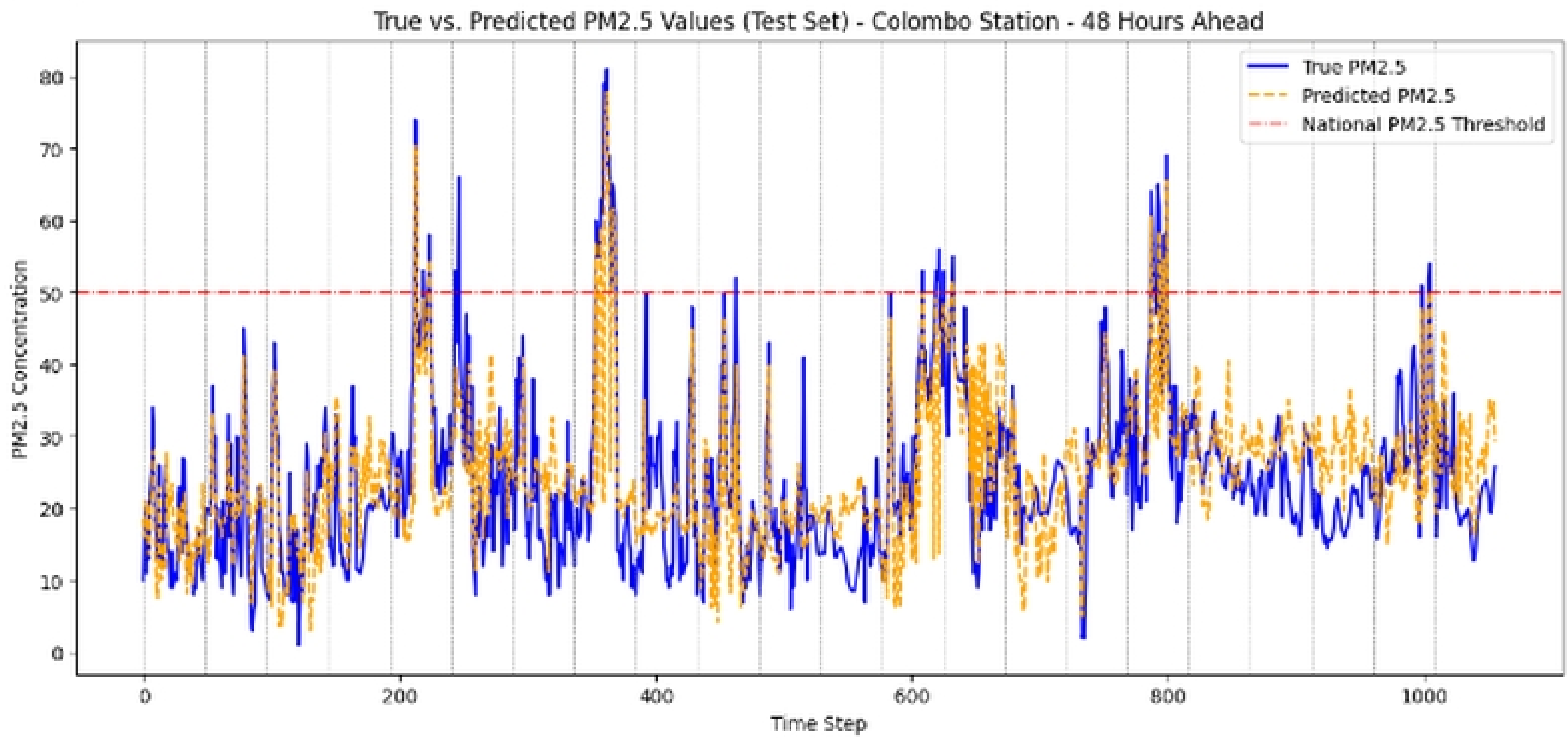
True vs. Predicted PM2.5 Values (Test Set) - Colombo Station - 48 Hours Ahead
True PM2.5
Predicted PM2.5
National PM2.5 Threshold
PM2.5 Concentration
Time Step

**(A)**



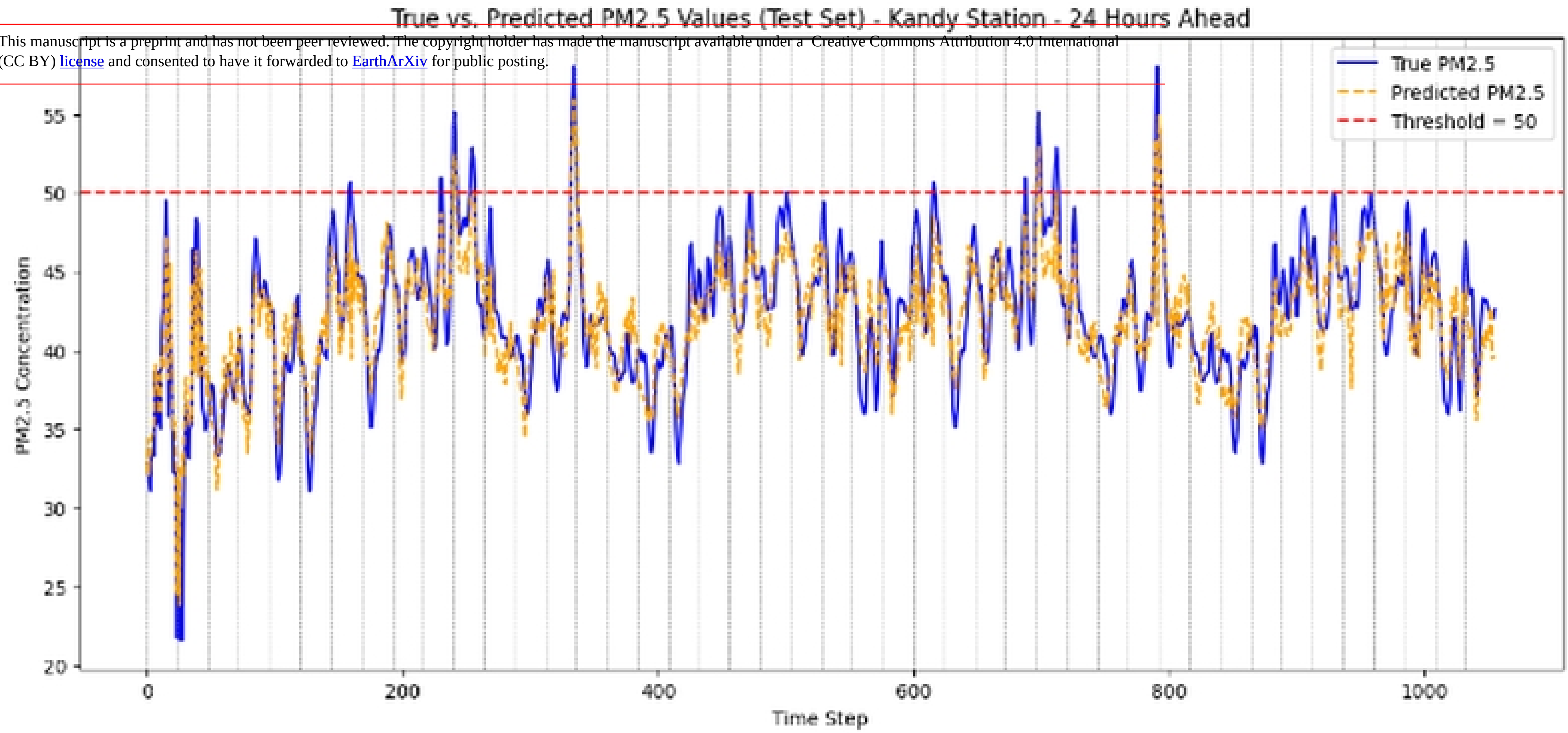
True vs. Predicted PM2.5 Values (Test Set) - Kandy Station - 24 Hours Ahead
True PM2.5
Predicted PM2.5
Threshold = 50
PM2.5 Concentration
Time Step
20
25
30
35
40
45
50
55
0
200
400
600
800
1000

**(B)**

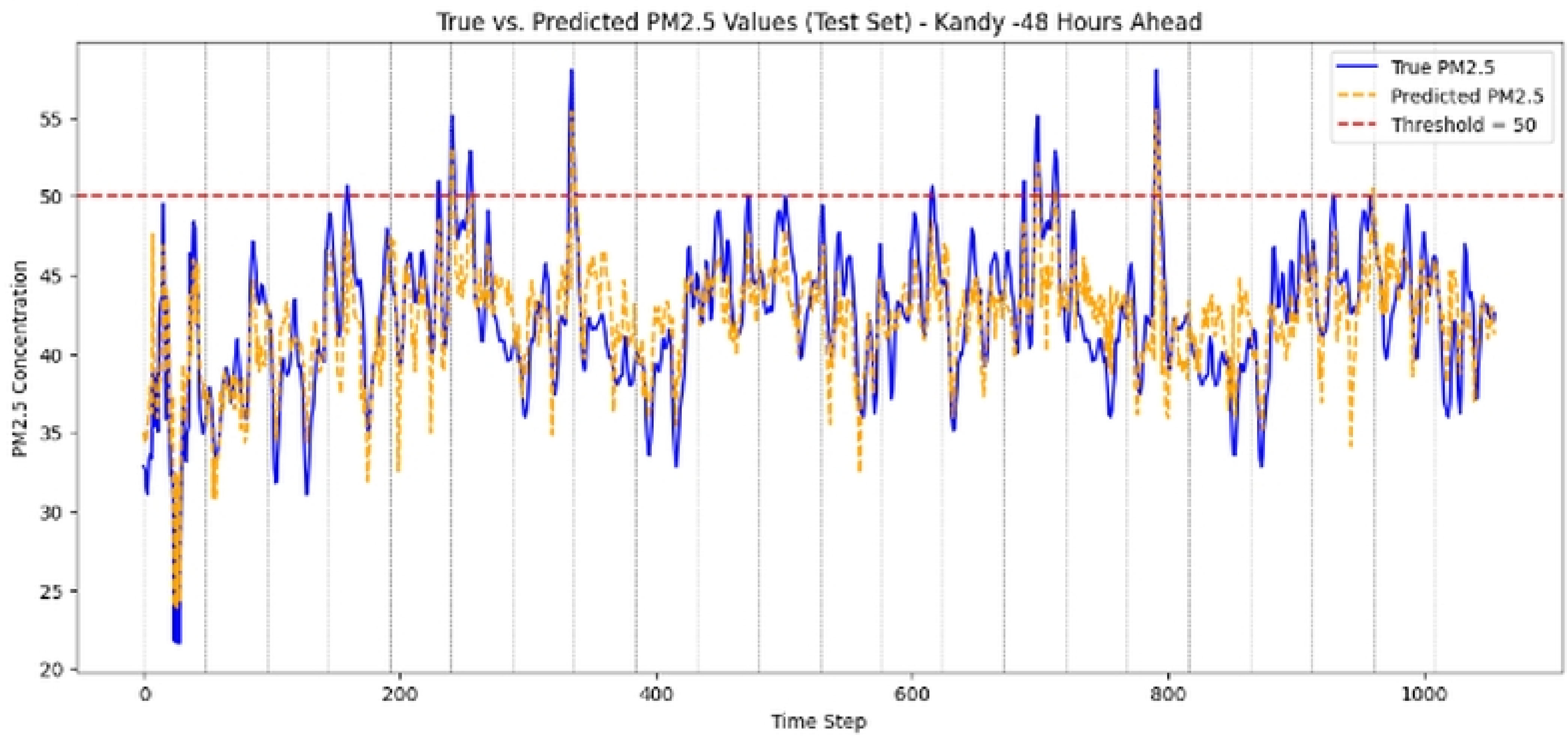
True vs. Predicted PM2.5 Values (Test Set) - Kandy -48 Hours Ahead
True PM2.5
Predicted PM2.5
Threshold = 50
PM2.5 Concentration
Time Step
20
25
30
35
40
45
50
55
0
200
400
600
800
1000

(A)

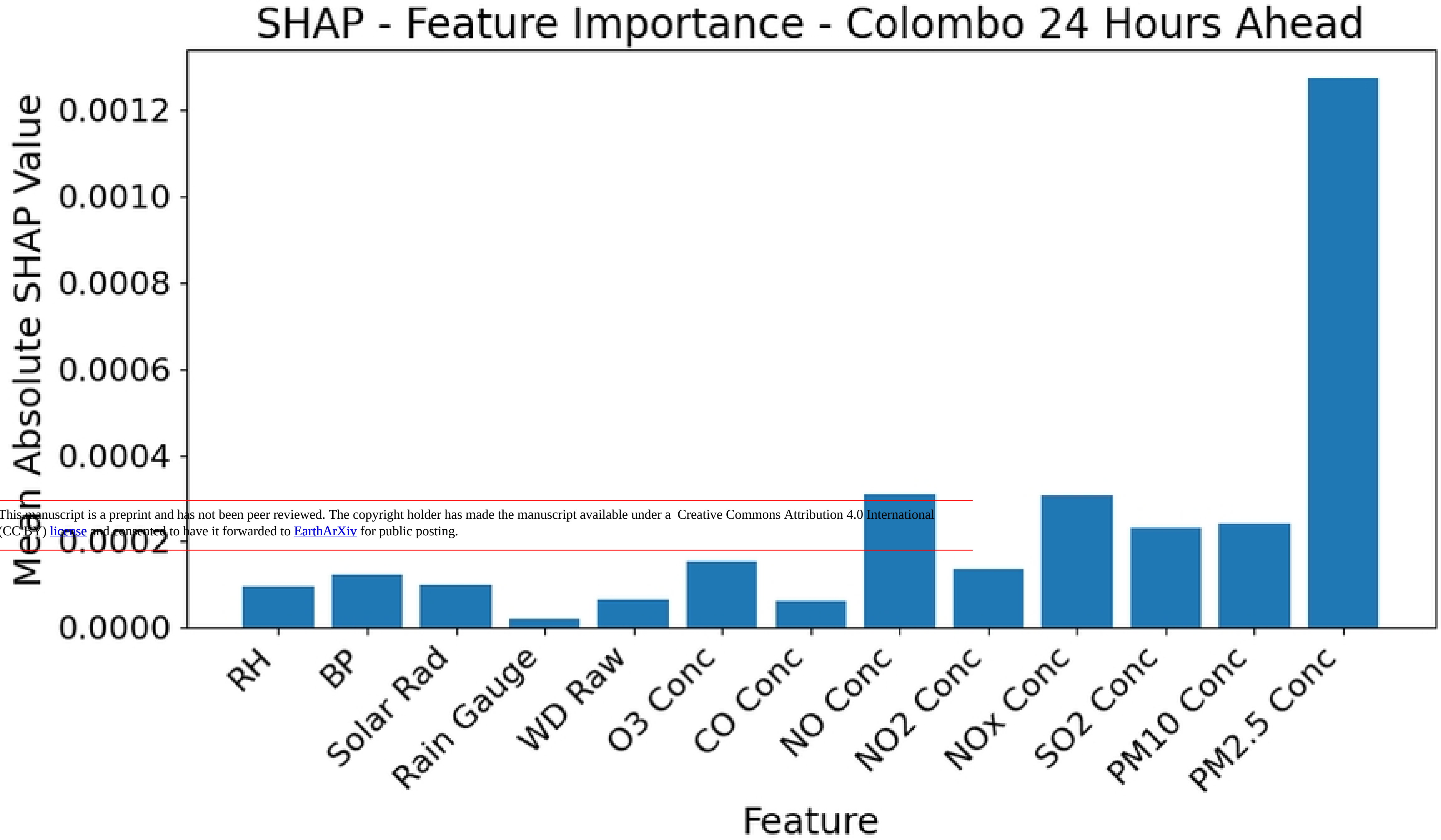
SHAP - Feature Importance - Colombo 24 Hours Ahead
Mean Absolute SHAP Value
0.0000
0.0002
0.0004
0.0006
0.0008
0.0010
0.0012
RH
BP
Solar Rad
Rain Gauge
WD Raw
O3 Conc
CO Conc
NO Conc
NO2 Conc
NOx Conc
SO2 Conc
PM10 Conc
PM2.5 Conc
Feature



(B)

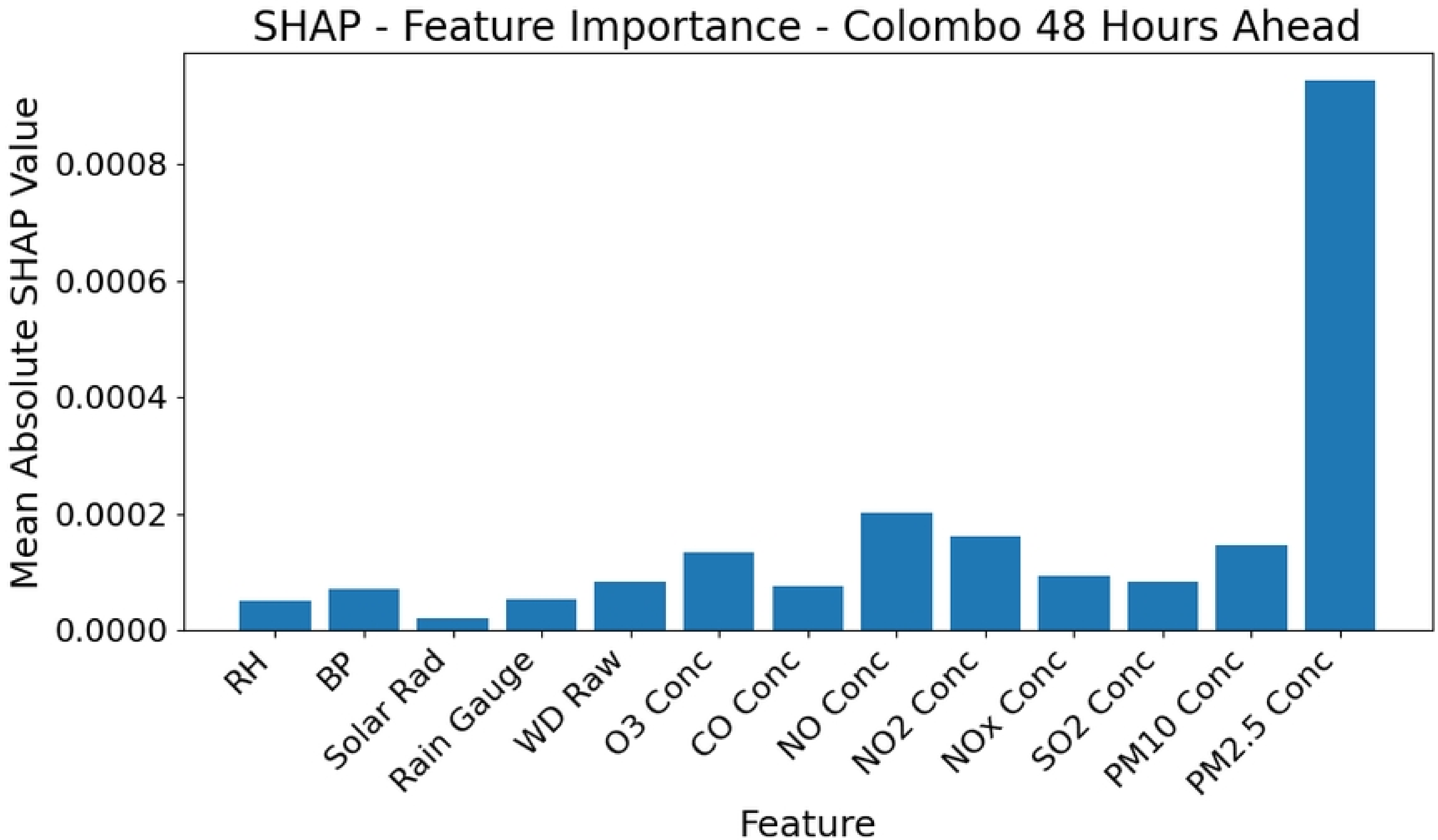
SHAP - Feature Importance - Colombo 48 Hours Ahead
Mean Absolute SHAP Value
0.0000
0.0002
0.0004
0.0006
0.0008
RH
BP
Solar Rad
Rain Gauge
WD Raw
O3 Conc
CO Conc
NO Conc
NO2 Conc
NOx Conc
SO2 Conc
PM10 Conc
PM2.5 Conc
Feature

(A)

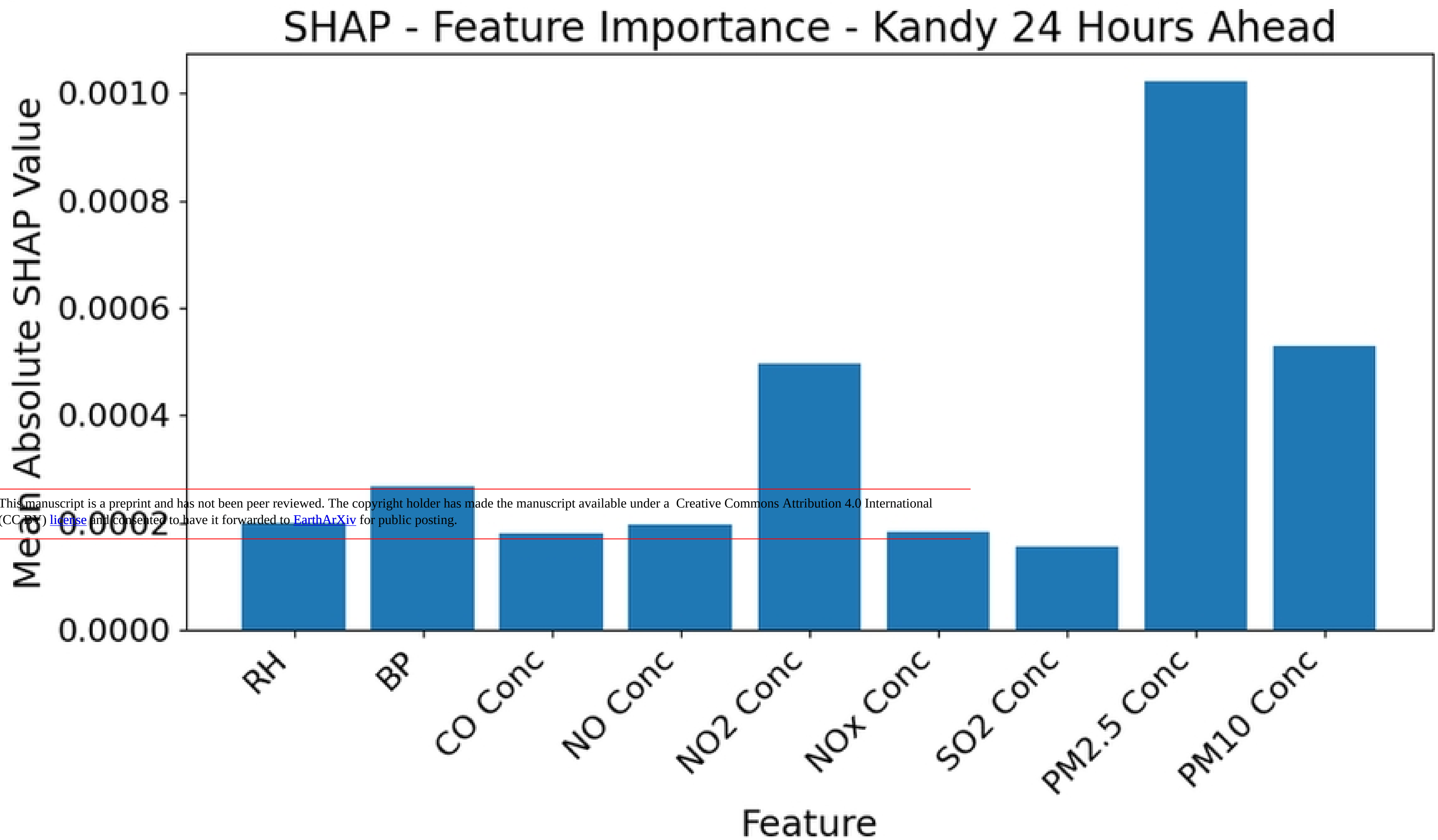

SHAP - Feature Importance - Kandy 24 Hours Ahead
Mean Absolute SHAP Value
0.0010
0.0008
0.0006
0.0004
0.0002
0.0000
RH
BP
CO Conc
NO Conc
NO2 Conc
NOx Conc
SO2 Conc
PM2.5 Conc
PM10 Conc
Feature




(B)

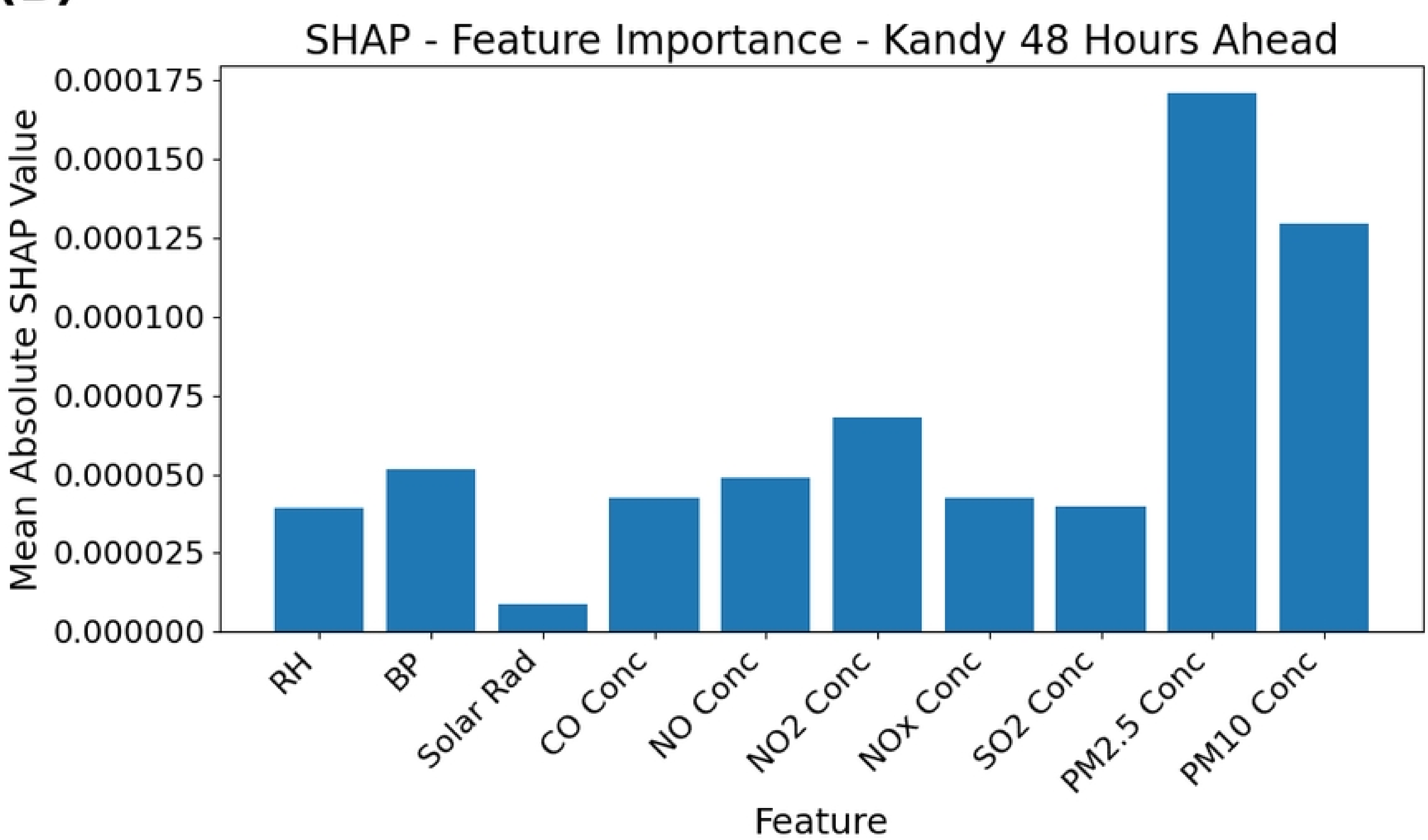

SHAP - Feature Importance - Kandy 48 Hours Ahead
Mean Absolute SHAP Value
0.000175
0.000150
0.000125
0.000100
0.000075
0.000050
0.000025
0.000000
RH
BP
Solar Rad
CO Conc
NO Conc
NO2 Conc
NOx Conc
SO2 Conc
PM2.5 Conc
PM10 Conc
Feature